Nano Energy 22 (2016) 490–498

Contents lists available at ScienceDirect

Nano Energy

journal homepage: www.elsevier.com/locate/nanoen

Communication

Hierarchical spheres constructed by defect-rich MoS_2/carbon nanosheets for efficient electrocatalytic hydrogen evolution

Linjing Yang [a], Weijia Zhou [a,*], Jia Lu [a], Dongman Hou [b], Yunting Ke [a], Guoqiang Li [b], Zhenghua Tang [a], Xiongwu Kang [a], Shaowei Chen [a,c,**]

[a] New Energy Research Institute, School of Environment and Energy, South China University of Technology, Guangzhou Higher Education Mega Centre, Guangzhou, Guangdong 510006, China
[b] State Key Laboratory of Luminescent Materials and Devices, Engineering Research Center on Solid-State Lighting and its Informationisation of Guangdong Province, South China University of Technology, 381 Wushan Road, Guangzhou 510641, China
[c] Department of Chemistry and Biochemistry, University of California, 1156 High Street, Santa Cruz, CA 95064, United States

ARTICLE INFO

Article history:
Received 12 November 2015
Received in revised form
20 January 2016
Accepted 28 February 2016
Available online 3 March 2016

Keywords:
Micro-emulsion
MoS_2/carbon
Hierarchical spheres
Active sites
Inverted molybdenum reaction

ABSTRACT

Highly active and stable MoS_2/carbon hierarchical spheres with abundant active edge sites were fabricated by a simple micro-emulsion procedure where PVP was used as the carbon source, and carbon disulfide as the sulfur source and oil phase in micro-emulsion to control the morphology of MoS_2. Hierarchical spheres of MoS_2/carbon with a diameter of ca. 500 nm were obtained and characterized by scanning and transmission electron microscopic measurements. With a high electrochemically accessible surface area and defect-rich MoS_2 nanosheets, the MoS_2/carbon hierarchical spheres exhibited an excellent electrocatalytic activity for hydrogen evolution reaction with a low onset potential of −103 mV (vs. RHE), small Tafel of 56.1 mV dec^{-1}, as well as extraordinary catalytic stability. The results were accounted for by the "inverted molybdenum reaction" that served as a novel way of regulating Mo catalytic sites of MoS_2 electrocatalysts.

1. Introduction

Hydrogen is a clean fuel and considered as a promising alternative for traditional fossil fuels in the future due to its high calorific value and environmental friendliness. Electrocatalytic hydrogen evolution reaction (HER) is one of the most important pathways to produce hydrogen that may efficiently store energy from renewable sources such as solar energy [1–3]. The most effective HER electrocatalysts up to now are based on noble metals, in particular, platinum [4,5]. However, the high costs severely limit their broad utilization in energy systems. Thus, there is an urgent need to develop effective alternative HER electrocatalysts that are of low costs and high abundance [6–15]. In recent years, low-cost MoS_2-based electrocatalysts have been attracting particular attention due to their similar hydrogen binding energy to that of Pt and hence high HER activity [16–19]. Yet, for MoS_2 that exhibits a well-known two-dimensional S–Mo–S sandwich structure, the preferentially exposed basal planes are actually the thermodynamically stable (002) planes rather than the active edge planes [20,21]. Both experimental and computational studies have shown that the HER activity of MoS_2 correlates with the number of catalytically active edge sites [22,23]. Therefore, to enhance the HER activity, a variety of strategies have been developed to engineer MoS_2 catalysts so as to increase the number of active sites, such as doping treatment [24–28], formation of vertically aligned layers [20,29], and loading on special substrates (porous Au, 3D Ni foam, graphene, MoO_2) [18,19,30–33]. For instance, Xie et al. reported that oxygen incorporation into MoS_2 led to dramatically enhanced HER activity [26]. The disordered structure offered abundant unsaturated sulfur atoms as active sites for HER, while the oxygen incorporation effectively regulated the electronic structure and further improved the intrinsic conductivity. In fact, doping treatment has been found to effectively enhance the HER activity of MoS_2, such as Cl [25], O [26], and N [28]. In addition, to further enhance the HER activity, a variety of MoS_2 structures have been prepared, for instance, nanosheets [23,34], nanobelts [35], nanoparticles [19,24], quantum dots [16], nanotubes [36], and microboxes [37]. However, to the best of our knowledge, hollow hierarchical nanospheres composed of MoS_2 nanosheets as electrocatalysts for HER have not been reported till now.

Herein, we describe a scalable pathway based on micro-emulsion to engineer structural defects on MoS_2 surfaces so as to

* Corresponding author.
** Corresponding author at: New Energy Research Institute, School of Environment and Energy, South China University of Technology, Guangzhou Higher Education Mega Centre, Guangzhou, Guangdong 510006, China.
E-mail addresses: eszhouwj@scut.edu.cn (W. Zhou), shaowei@ucsc.edu (S. Chen).

http://dx.doi.org/10.1016/j.nanoen.2016.02.056
2211-2855/

expose active edge sites and propose a new mechanism based on "inverted molybdenum reaction" to account for the HER activity. Micro-emulsion has been used as an effective method to synthesize various hollow structures via interfacial reactions between an oil phase and a water phase, such as CoS_2 [38], Ag_2S [39], CuS [40], and silica [41]. Experimentally, to achieve a defect-rich structure, CS_2 was used not only as the oil phase to control the morphology of the products, but also as the sulfur sources to synthesize MoS_2 nanosheets. Then, thermal treatment at 35 °C under an Ar atmosphere produced a small quantity of carbon from PVP to form MoS_2/carbon compound electrocatalysts (C–MoS_2). Because the hierarchical spheres composed of defect-rich C MoS_2 nanosheets displayed the high electrochemically surface area and exposed the abundant active edge sites, leading to an excellent electrocatalytic activity for HER with a low onset potential of −103 mV (vs. RHE), a small Tafel slope of 56.1 mV dec^{-1}, a low overpotential of 159 mV at the current density of 10 mA cm^{-2}, and excellent catalytic stability.

2. Experimental

2.1. Chemicals

PVP (MW=1,300,000 Da), carbon disulfide (CS_2), ethylenediamine ($C_2H_8N_2$), ammonium molybdate ($(NH_4)_2MoO_4 \cdot 2H_2O$), sodium molybdate ($Na_2MoO_4 \cdot 2H_2O$) and thioacetamide ($C_2H_5NS$) were purchased from Sinopharm Chemical Reagents Beijing Co. All reagents were of analytical grade and used without further treatment. Deionized water was purified using a Milli-Q system (Millipore, Billerica, USA).

2.2. Preparation of MoS_2/carbon (C–MoS_2) hierarchical spheres

Briefly, ammonium molybdate (1 mmol) was dispersed in deionized water (30 mL) under continuous stirring. Then, ethylenediamine (0.5 mL), PVP (MW 1,300,000, 0.06 g), and CS_2 (1 mL) were added to the solution and sonicated for 30 min. The mixture was then transferred to a 50 mL Teflon-lined autoclave, heated at 200 °C for 24 h, and cooled naturally to room temperature. The resulting dark precipitation was collected, washed with ethanol and dried in vacuum at 80 °C for 12 h, affording PVP/MoS_2 hierarchical spheres. The samples were then pyrolyzed at 350 °C for 2 h under an Ar atmosphere to obtain C–MoS_2 hierarchical spheres. MoS_2 hierarchical spheres were also prepared in the similar fashion but without the addition of PVP. In addition, samples were prepared by adding different amounts of CS_2 (0.5 mL, 0.7 mL, 1 mL and 20 mL).

2.3. Preparation of MoS_2 nanosheets alone

Typically, 30 mg $Na_2MoO_4 \cdot 2H_2O$ and 60 mg C_2H_5NS were dissolved in 20 mL of deionized water to form a solution, which was then transferred to a Teflon-lined stainless steel autoclave and heated in an electric oven at 200 °C for 24 h. Black MoS_2 nanosheets was harvested after centrifugation and dried at 80 °C for 12 h.

2.4. Characterization

Field-emission scanning electron microscopic (FESEM, Model JSM-7600F) measurements were employed to characterize the morphologies of the obtained samples. Transmission electron microscopic (TEM) measurements were carried out with a JOEL JEM 2100F microscope. Powder X-ray diffraction (XRD) and small-angle XRD patterns of the samples were recorded with a Bruke D8 Advance powder X-ray diffractometer with Cu Kα (λ=0.15406 nm) radiation. X-ray photoelectron spectroscopic (XPS) measurements were performed using a PHI X-tool instrument (Ulvac-Phi). Raman spectra were recorded on a RENISHAW inVia instrument with an Ar laser source of 488 nm in a macroscopic configuration. BET surface area was determined by Micromeritics ASAP 2010 with nitrogen adsorption at 77 K and the Barrett–Joyner–Halenda (BJH) method. The content of carbon in C–MoS_2 sample was measured by the high frequency infrared ray carbon sulphur analyser (QL-HW2000B).

2.5. Electrochemistry

Electrochemical measurements were performed with an electrochemical workstation (Solartron Analytical 1287+1260) in a 0.5 M H_2SO_4 aqueous solution. A saturated calomel electrode (Hg/Hg_2Cl_2 in saturated KCl) and a carbon cloth were used as the reference and counter electrode, respectively. A calculated amount of sample was loaded on a glassy carbon electrode (GCE) which was used as the working electrode. Experimentally, 5 mg of the respective catalyst powders was dispersed in 1 mL of 1:1 (v/v) water/ethanol mixed solvents with 40 μL of a Nafion solution under ultrasonication for 30 min. 5 μL of the resulting solution was dropcast onto the glassy-carbon disk by a microliter syringe and dried at room temperature.

Polarization curves without ohmic compensation were acquired by sweeping the potential from 0 to −0.8 V (vs. SCE) at a potential sweep rate of 5 mV s^{-1}. Electrochemical impedance spectroscopy (EIS) was carried out with an amplitude of 10 mV and frequency range from 100 kHz to 0.01 Hz. The main arc in the EIS spectra was fitted using a simplified Randles equivalent circuit, which consisted of a resistance (Rs, electrical electronic conductivity of electrodes), a charge-transfer resistance (Rct, interface electrocatalytic reaction between electrode and electrolyte) and a constant phase element (CPE), and the fitting parameters were estimated through the application of the Levenberg–Marquardt minimization procedure. Cyclic voltammetry (CV) was used to probe the electrochemical double layer capacitance at nonfaradaic potentials as a means to estimate the effective electrode surface area. The accelerated stability tests were performed in 0.5 M H_2SO_4 at room temperature by potential cycling between +0.1 and −0.5 V (vs. SCE) at a sweep rate of 100 mV s^{-1} for 1000 cycles. Current–time responses were monitored by chronoamperometric measurements for up to 12 h at the applied potential of −0.157 V (vs. RHE).

3. Results and discussion

The synthesis of C–MoS_2 hierarchical spheres was summarized in Scheme 1. Experimentally, CS_2 formed stable micro-emulsion with PVP in water, and served both as the sulfur source and as the soft template during hydrothermal treatment. Prolonged reaction time formed the robust nanosheet-like shells composed of MoS_2 nanosheets at the CS_2/water interface. This may be accounted for by the "inverted molybdenum reaction" mechanism, where S ions produced from CS_2 diffused into the aqueous phase and multiple Mo ions competed in reaction with the same S ion, forming Mo–S–Mo compounds with more S defects. As a contrast, water-soluble Mo ions can not diffuse into oil phase of CS_2. So, compared with traditional Mo template, the "inverted molybdenum reaction" can produce more S defects to enhance the HER activity (Fig. S1). Excessive encapsulated CS_2 droplets might be readily removed by solvent washing, whereas the MoS_2 shells would be kept intact, leading to the formation of a hollow structure. At the same time, a small quantity of carbon was converted from PVP via thermal treatment at 350 °C under an Ar

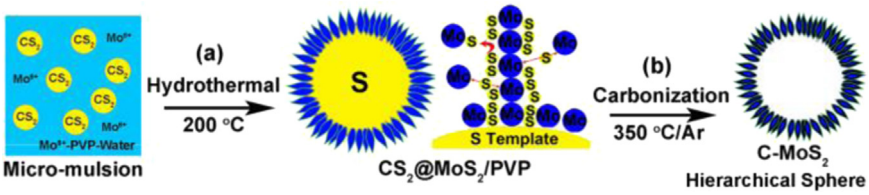

Scheme 1. Schematic illustration of the synthesis of C–MoS_2 hierarchical spheres.

atmosphere and formed C–MoS_2 hierarchical spheres.

SEM measurements indeed showed that the resulting samples consisted of hierarchical spheres with a diameter of 400–600 nm (Fig. 1a), and the hierarchical sphere was decorated with a number of vertically aligned nanosheets (Fig. 1b). Some cracked spheres marked by circles in Fig. 1a were also observed, implying the possible hollow structure. Note that without PVP, only irregularly and non-uniformly shaped MoS_2 was produced (Fig. S2). However, too much PVP increased the size of obtained MoS_2 spheres and lead to the more uniform and dense structure (Fig. S3). Fig. 1c shows a representative TEM image of the C–MoS_2 hierarchical spheres, where one can see that MoS_2 nanosheets grew outwards from the inner core forming a flaky structure. Some hollow spheres with distinct color contrast between the edge and the center were also observed in inset of Fig. 1c. This suggests that the sulfur source likely diffused from the interior to the CS_2–water interface where the growth of MoS_2 nanosheets occurred. Nitrogen adsorption–desorption isotherms (Fig. S4) were then acquired to determine the surface area and pore-size distribution, where one can see that the hierarchical spheres entailed well-defined

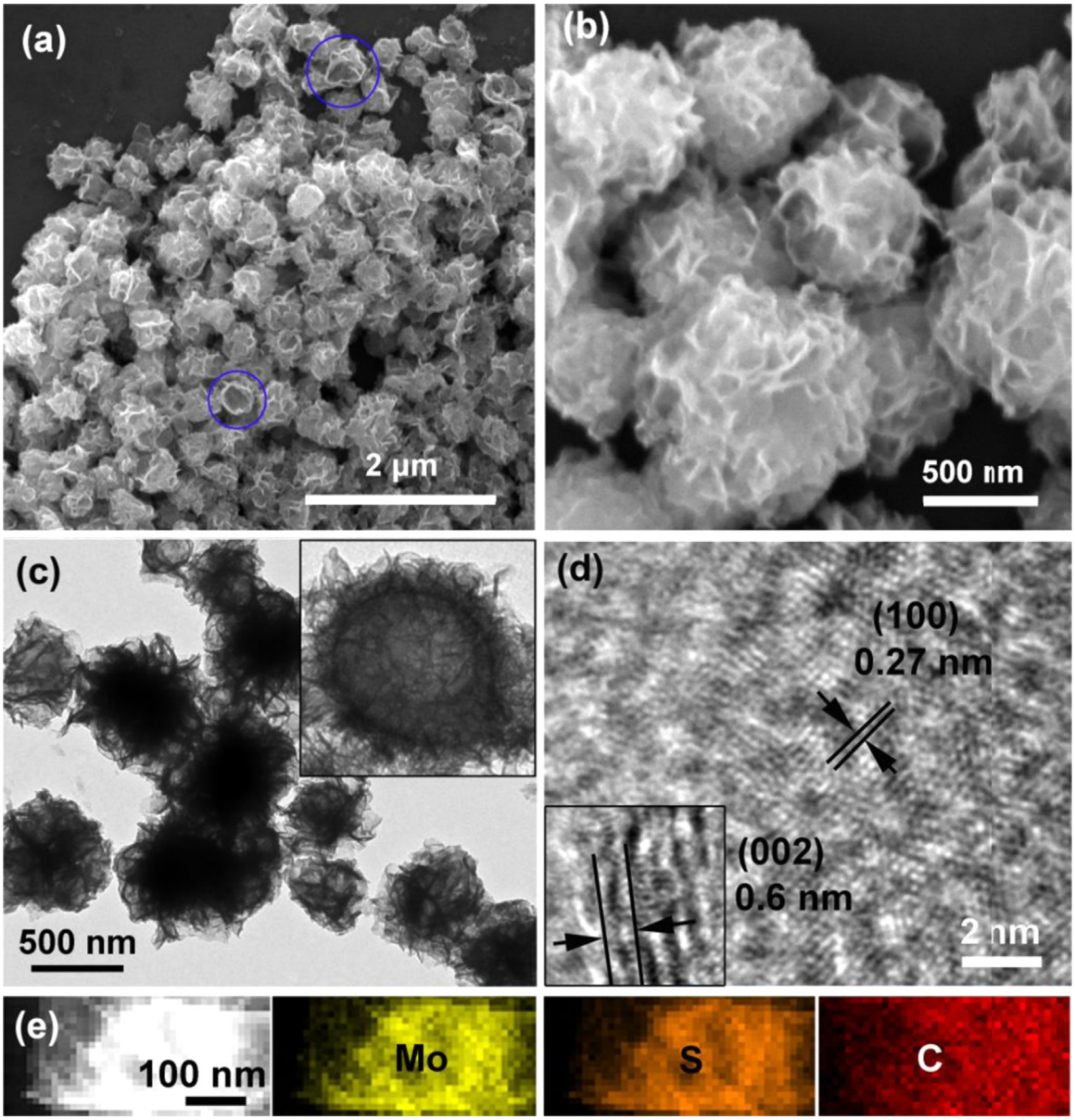

Fig. 1. (a, b) SEM and (c, d) (HR)TEM images of C–MoS_2 hierarchical spheres, and (e) the corresponding EDX elemental mapping images of Mo, S and C.

mesoporosity with a pore-size distribution of about 50 nm. This is consistent with the TEM results, where the pores were likely generated by the soft templates of CS_2. The surface area of the C–MoS_2 hierarchical spheres was estimated to be 43.7 $m^2 g^{-1}$, almost twice that of MoS_2 nanosheets alone (22.8 $m^2 g^{-1}$).

Indeed, in high-resolution TEM measurements (Figs. 1d and S5a), one can see abundant exposed edges of the MoS_2 nanosheets with a thickness of ca. 4 nm, corresponding to a thickness of 4–7 layers. The diffraction rings corresponded to the lattice planes of (100) and (110) confirmed that the polycrystalline C–MoS_2 possess a large number of defects (Fig. S5b). From Fig. 1d, lattice fringes can also be observed and the spacings of 0.27 nm and 0.60 nm are consistent with the (100) and (002) crystalline planes of MoS_2, respectively. Elemental mapping studies further confirmed the homogeneously distributed Mo, S and C elements, in the C–MoS_2 hierarchical spheres (Fig. 1e), implying the PVP as a surfactant regulated the nucleation and growth of MoS_2 nanosheets.

The as-synthesized C–MoS_2 hierarchical spheres were then examined by XRD measurements. The XRD patterns in Fig. S6 attest the purity of the hierarchical spheres, as evidenced by the characteristic diffraction peaks at 33.5° and 58.3° for MoS_2 (100) and (110) (JCPDS card no. 37-1492), respectively. No other diffraction peaks were detected. The absence of the (00l) diffraction in the XRD patterns clearly showed that the long-range stacking order of the MoS_2 nanosheets along the *c* axis was destroyed. In Raman spectroscopic measurements (Fig. S7), the very weak vibrational bands at 1350.4 and 1593.8 cm^{-1} (the intensity was multiplied by a factor of 10) were observed after the sample was thermally annealed at 350 °C under an Ar atmosphere. These were consistent with the characteristic D and G vibrational bands of graphitic carbon that was likely produced from carbonization of PVP. The ratio of the peak intensity (I_D/I_G) was estimated to be 2.05, suggesting weak sp^2 hybridization of the carbon and abundant structural defects.

XPS measurements were then carried out to examine the chemical composition and bonding structures of the C–MoS_2 hierarchical spheres. The survey spectrum in Fig. 2a confirmed the presence of Mo, S, C and O elements in the samples. The high-resolution scan of the C 1s electrons was depicted in Fig. 2b, where deconvolution yields a peak at 284.5 eV characteristic of sp^2 carbon, another one at 285.3 eV for C–S and a third one at 288.5 eV for C–O, which illustrated the interfacial effect between carbon and MoS_2 in C–MoS_2 hierarchical spheres. For Mo3d electrons (Fig. 2c), two prominent peaks can be identified at 228.9 eV and 232.3 eV, consistent with the $3d_{5/2}$ and $3d_{3/2}$ electrons of Mo(IV), respectively [28,42]. The S2s electrons can also be seen at 235.0 eV. For the S2p electrons (Fig. 2d), two peaks can be resolved at 161.9 eV and 163.7 eV that corresponded to the $2p_{3/2}$ and $2p_{1/2}$ electrons of S(II), respectively. Furthermore, based on the integrated peak areas of Mo and C-S, the atomic content of C in the hierarchical spheres was estimated to be ~4.9 at%, which was lower than that (9.49 wt%) obtained by the high frequency infrared ray carbon sulhur analyser due to the different measurement mechanisms. In contrast, the XPS survey spectrum of MoS_2 nanosheets obtained from TAA or CS_2 without PVP showed no peaks for C–O and C–S (Fig. S8), which illustrated the carbon in C–MoS_2 possibly from carbonization of PVP.

The electrocatalytic HER activities of C–MoS_2 hierarchical

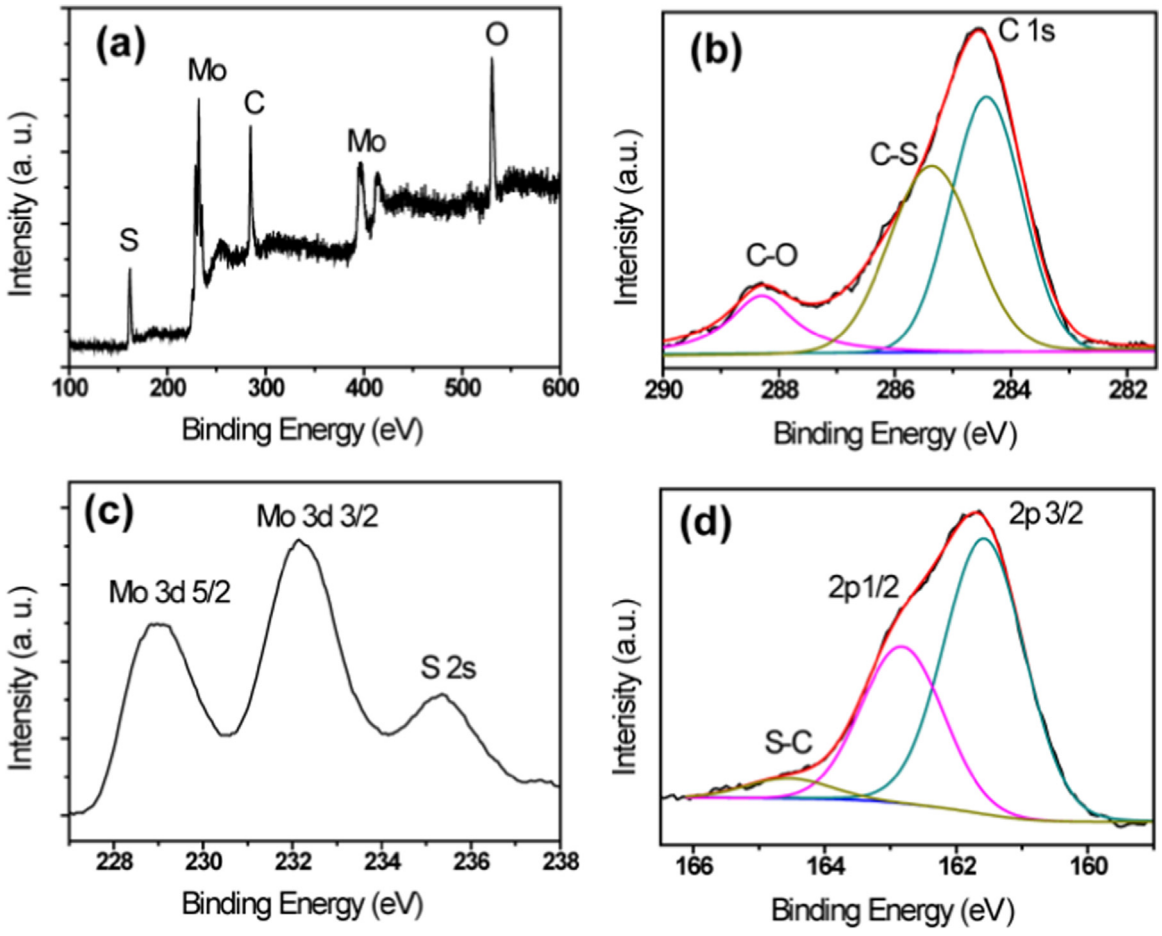

Fig. 2. (a) XPS survey spectrum and high-resolution scans of (b) C 1s, (c) Mo 3d, and (d) S 2p electrons of C–MoS_2 hierarchical spheres. Black curves are experimental data and colored curves are deconvolution fits.

spheres were then investigated in 0.5 M H_2SO_4 solution by linear sweep voltammetry (LSV) using a three-electrode setup. Fig. 3a depicted the polarization curves for a glassy carbon electrode (GCE) modified with 20 wt% Pt/C, C–MoS_2 hierarchical spheres, PVP/MoS_2 hierarchical spheres and MoS_2 nanosheets, respectively. One can see that at all electrodes, as the electrode potential swept to sufficiently negatively potentials, nonzero cathodic currents started to emerge, suggesting apparent HER activity in the electroreduction of protons into hydrogen. Among these, C–MoS_2 hierarchical spheres showed a small onset potential of −103 mV and an overpotential (η) of 0.159 mV at the current density (j) of 10 mA cm^{-2}. While it remained subpar as compared to that of 20 wt% Pt/C (with an onset potential of only −4 mV vs. RHE), this performance was markedly better than that of MoS_2 nanosheets alone (SEM image was shown in Fig. S9), which exhibited an onset potential of −167 mV, implying that the hierarchical structure played an important role in enhancing the HER activity likely due to the increased exposure of edge active sites. Indeed, from Fig. 3b

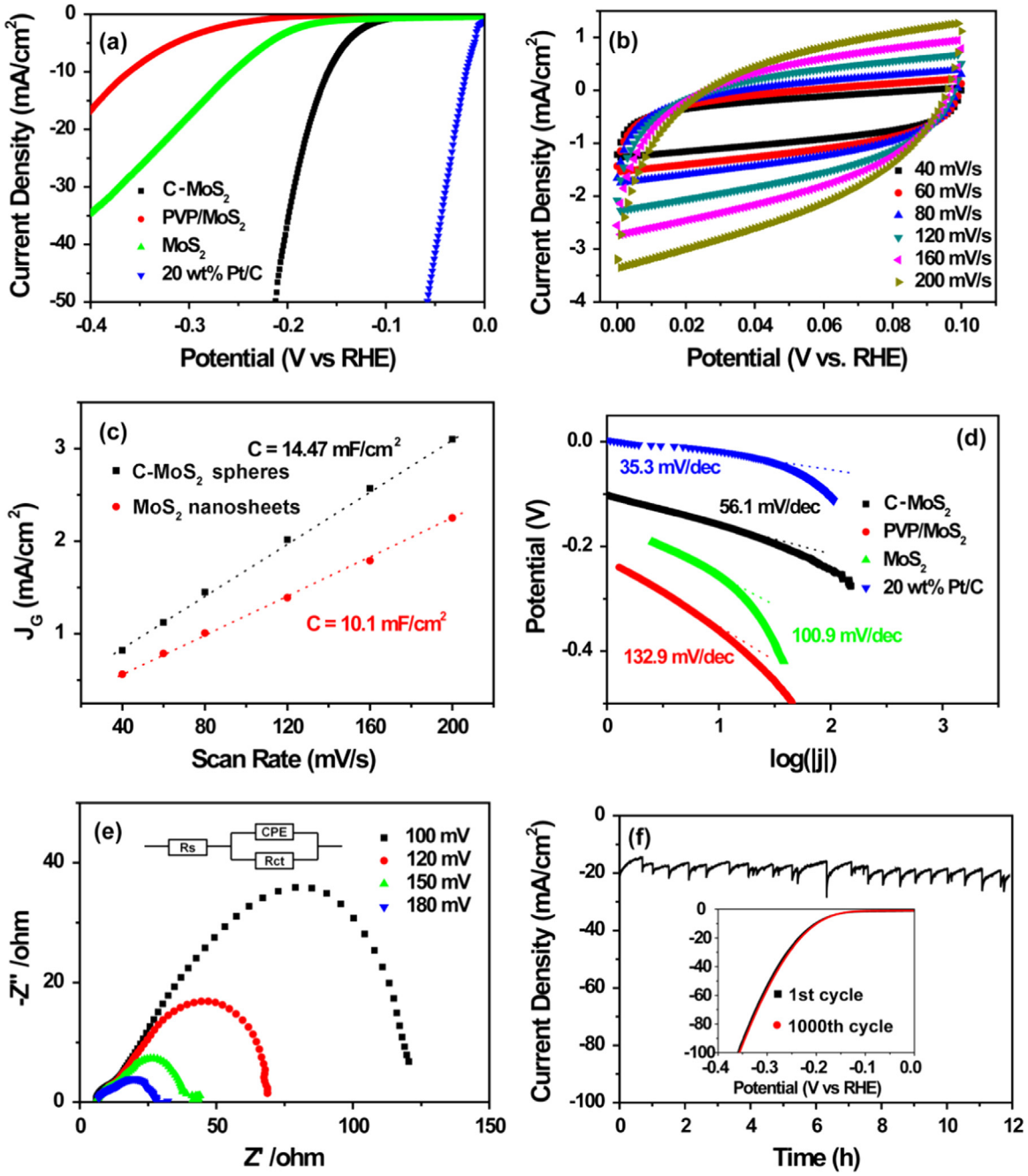

Fig. 3. (a) Polarization curves (iR uncorrected) for HER in 0.5 M H_2SO_4 of 20 wt% Pt/C, C–MoS_2 hierarchical spheres, PVP/MoS_2 hierarchical spheres, and MoS_2 nanosheets, respectively. Potential sweep rate is 5 mV s^{-1}. (b) Cyclic voltammograms within the range of 0 to +0.1 V where no faradaic reactions occurred. (c) Variation of double-layer charging currents at +0.05 V with potential scan rate. Symbols are experimental data acquired from panel (b), and dotted line is linear regression. (d) Corresponding Tafel plots derived from (a). (e) Nyquist plots and the equivalent circuit of C–MoS_2 hierarchical spheres at various HER overpotentials in 0.5 M H_2SO_4. (f) Current-time plots of the C–MoS_2 hierarchical spheres at the applied potential of −0.157 V (vs. RHE). The inset is HER polarization curves for C–MoS_2 hierarchical spheres before and after 1000 cycles in the stability test.

and c, one can see that the C–MoS_2 hierarchical spheres modified electrode possessed a higher double layer capacitance (14.47 mF cm^{-2}) than that (10.1 mF cm^{-2}) of MoS_2 nanosheets alone. Even after being corrected by electrochemical surface area, the HER performance of C–MoS_2 hierarchical spheres was still better than that of MoS_2 nanosheets (Fig. S10), implying that electrochemical surface area was not the only reason for enhanced HER activity of C–MoS_2 hierarchical spheres. It is worth noting that the current density of C–MoS_2 hierarchical spheres (−36.1 mA cm^{-2}) at −0.2 V was much higher than that (−3.1 mA cm^{-2}) of PVP/MoS_2 hierarchical spheres (Fig. 3a). Note that they possess the same hierarchical structure (Fig. S11), implying that the carbon converted from PVP via thermal treatment also led to the enhanced HER activity. So, the enhanced electrocatalytical activity for HER from the C–MoS_2 hierarchical spheres was probably due to (i) the hierarchical sphere with possible hollow structure possessed a high electrochemical area. Note that without PVP, only irregularly and non-uniformly shaped MoS_2 was produced (Fig. S2). (ii) the defect-rich structure of MoS_2 was obtained by "inverted molybdenum reaction" (Scheme 1 and Fig. S1), in which, S defects were formed by competing between multi-Mo ions with the same S ion and (iii) the efficient heterostructures between MoS_2 and carbon from PVP reduced the resistance (Rs) from 9.97 Ω of MoS_2 to 6.91 Ω of C–MoS_2 (Fig. S12). In addition, the carbon also possibly introduced more defects into MoS_2, which was confirmed by HRTEM (Figs. 1e,f and S5) and XPS (Fig. 2) results.

The linear portions of the Tafel plots were fitted to the Tafel equation ($\eta = b \log j + a$, where j is the current density and b is the Tafel slope), yielding Tafel slopes of 56.1 mV dec^{-1}, 100.9 mV dec^{-1}, 132.9 mV dec^{-1} and 35.3 mV dec^{-1} for C–MoS_2 hierarchical spheres, MoS_2 nanosheets, PVP/MoS_2 hierarchical spheres and 20 wt% Pt/C, respectively (Fig. 3d). A lower Tafel slope suggests a smaller activation energy for HER, which means a lower overpotential is required to generate a certain current density. According to the classic theory on the mechanism of hydrogen evolution, the overall HER reaction occurring at C–MoS_2 hierarchical spheres in acidic media may proceed via a discharge step (Volmer-reaction, 120 mV dec^{-1}) followed by either an ion and atom reaction (Heyrovsky reaction, 40 mV dec^{-1}) or a combination reaction (Tafel reaction, 30 mV dec^{-1}). Generally, the initial discharge step to form adsorbed hydrogen is fast, while the following hydrogen desorption process is the typical rate-limiting step. Such a HER performance of C–MoS_2 hierarchical spheres (onset potential of −103 mV, Tafel slope of 56.1 mV dec^{-1}) is better than or comparable to those of leading Mo-based HER catalysts, such as semimetallic MoS_2 ultrathin nanosheets (−130 mV, 69 mV dec^{-1}) [43], MoS_2 nanoflower-decorated reduced graphene oxide paper (−190 mV, 95 mV dec^{-1}) [44], edge-terminated molybdenum disulfide (−103 mV, 49 mV dec^{-1}) [45], ultrathin WS_2 nanoflakes (−100 mV, 48 mV dec^{-1}) [46], MoS_2 formed on mesoporous graphene (–100 mV, 42 mV dec^{-1}) [17], few-layered metallic $WS_{2(1-x)}Se_{2x}$ nanoribbons (–173 mV with 10 mA cm^{-2}, 68 mV dec^{-1}) [47], monolayer MoS_2/WS_2 quantum dots (–120 mV, 69 mV dec^{-1}) [48], which were summarized in Table S1.

The HER kinetics at the electrode/electrolyte interface was further investigated by electrochemical impedance spectroscopy (Fig. 3e). The charge transfer resistance (Rct) is related to the electrocatalytic kinetics, and a lower value corresponds to a faster reaction rate, which can be quantified from the diameter of the semicircle in the low frequency zone. It can be seen that the Rct values of C–MoS_2 hierarchical spheres modified-GCE decreased significantly with increasing overpotentials, from 123.2 Ω at 100 mV to only 21.4 Ω at 180 mV, suggesting fast electron transfer and favorable HER kinetics at the electrolyte interface.

Furthermore, the cycle performance of C–MoS_2 hierarchical spheres was investigated, as depicted in the polarization curves in Fig. 3f. Inset to Fig. 3f showed that, even after continuous operation of 1000 potential cycles, the catalyst showed similar i–V curves with a negligible decay of the cathodic currents, indicating long-term viability under the operating conditions. To further verify the stability of C–MoS_2 hierarchical spheres for HER, the current-time plot was acquired at the potential of −0.157 V (vs. RHE) for 12 h of continuous operation. The catalytic current remained largely unchanged, indicating strong durability of the C–MoS_2 hierarchical spheres for HER in 0.5 M H_2SO_4. The periodic current fluctuation in current-time curve was attributed to the accumulation and stripping of H_2 gas bubbles produced by electrolysis of water. After the i–t testing for 12 h, the hierarchical C–MoS_2 spheres were also observed by TEM as shown in Fig. S13, which confirmed that the structure stability as well as catalytic stability. This is because that the catalytic reaction for HER is the interface reaction, which is related to the conductivity and surface atoms of electrocatalysts. In fact, no significant change in hierarchical C–MoS_2 spheres was confirmed by XPS (Fig. S14) and electrochemical impedance (Fig. S15) results after the i–t testing for 12 h.

Note that the CS_2 amount may significantly impact the morphologies and HER performance of C–MoS_2 hierarchical spheres. With the increase of CS_2 (0.5 mL, 0.7 mL, 1 mL and 20 mL), the C–MoS_2 hierarchical spheres gradually become rough and fluffy, as observed by SEM measurements (Fig. 4a-c). For instance, for the sample obtained by the addition of 0.5 mL CS_2, the C–MoS_2 hierarchical spheres were solid without a hollow structure (Fig. 4d). In contrast, for the samples obtained by 0.7 mL and 1 mL CS_2, the hollow structures were observed (Figs. 1 and 4e). For the sample obtained by more CS_2 (20 mL), C–MoS_2 hierarchical spheres became messy and disordered (Fig. 4c). TEM measurements (Fig. 4f) also confirmed that C–MoS_2 hierarchical spheres obtained by 20 mL CS_2 were fragile, and only some fragments were observed after ultrasonic treatment. Thus the morphology of the C–MoS_2 indeed strongly depended on the ratio of CS_2 to H_2O due to the formation mechanism of micro-emulsion. The BET surface area and pore-size distribution of C–MoS_2 samples obtained by different CS_2 amount also approved the above conclusion (Fig. S16). The lower BET values of C–MoS_2 synthesized by 0.5 ml CS_2 and 20 ml CS_2 were 6.05 m^3/g and 8.6 m^3/g, respectively. Fig. S16b showed the C–MoS_2 synthesized by 0.5 ml CS_2 was solid without hollow structure. The electrocatalytic HER activities of these C–MoS_2 samples were then investigated and compared in 0.5 M H_2SO_4 solution (Fig. 4g). The required overpotentials to generate a catalytic current density of 10 mA cm^{-2} increased in the order of 1 mL (−0.159 V) < 0.7 mL (−0.224 V) < 20 mL (−0.246 V) < 0.5 mL (−0.364 V), in agreement with the trend of electrochemical surface area of 1 mL (14.47 mF cm^{-2}) > 0.7 mL (11.96 mF cm^{-2}) > 20 mL (3.66 mF cm^{-2}) > 0.5 mL (0.93 mF cm^{-2}) (Fig. 4h). However, after being corrected by electrochemical surface area, the C–MoS_2 hierarchical spheres synthesized by 1 mL CS_2 still possessed the best HER performance (Fig. S17), implying that electrochemical surface area was not the only reason for enhanced HER activity, the different ratio of CS_2 to H_2O also possibly regulated more catalytic sites of hierarchical spheres of C–MoS_2 for HER.

4. Conclusions

In summary, C–MoS_2 hierarchical spheres with a high surface area and abundant defects were prepared by a simple microemulsion with PVP as the carbon source and CS_2 as the sulfur source. SEM, TEM, XPS and EDX measurements confirmed the formation of hierarchical structures composed of C–MoS_2 nanosheets with abundant defects. The obtained C–MoS_2

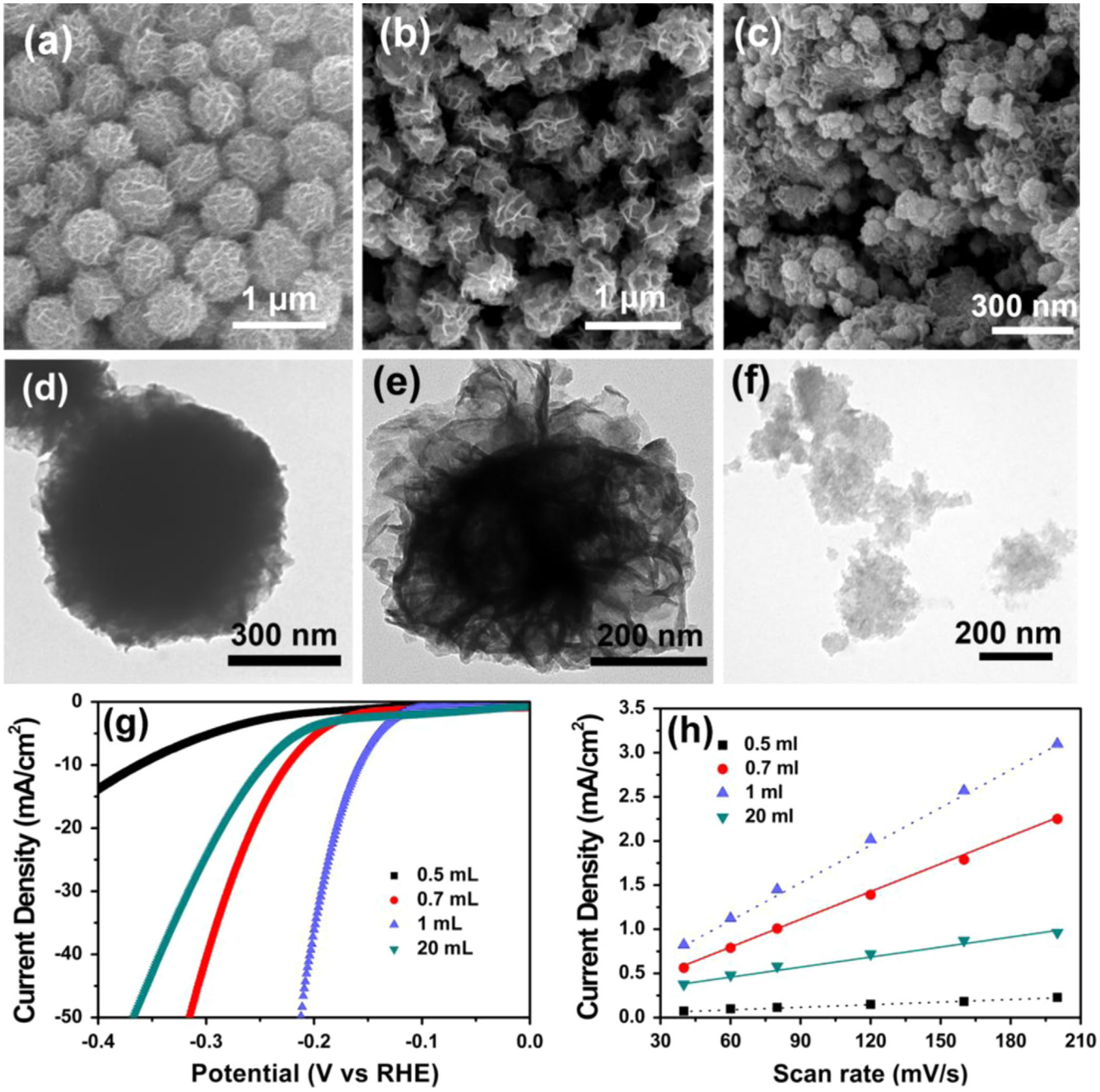

Fig. 4. SEM and TEM images of C–MoS_2 hierarchical spheres obtained by adding the different amount of CS_2: (a, d) 0.5 mL, (b, e) 0.7 mL and (c, f) 20 mL. (g) Polarization curves (iR-uncorrected) and (h) electrochemical surface areas of MoS_2 hierarchical spheres obtained by the addition of different amounts of CS_2.

hierarchical spheres exhibited a high HER activity with a low onset potential of − 103 mV (vs. RHE), an overpotential of 159 mV at the current density of 10 mA cm^{-2}, and high electrochemical surface area (14.47 mF cm^{-2}). A small Tafel slope of 56.1 mV dec^{-1} indicated a Volmer-Heyrovsky mechanism for the HER involved. The results suggested that the "inverted molybdenum reaction" might provide a novel method to regulate Mo catalytic sites on the surface of MoS_2 electrocatalysts.

Acknowledgments

This work was supported by the National Recruitment Program of Global Experts, Zhujiang New Stars of Science & Technology (2014J2200061), Project of Public Interest Research and Capacity Building of Guangdong Province (2014A010106005), the Fundamental Research Funds for the Central Universities (D2153880) and the National Natural Science Foundation of China (51502096).

Appendix A. Supplementary material

Supplementary data associated with this article can be found in the online version at http://dx.doi.org/10.1016/j.nanoen.2016.02.056.

References

[1] J. Liu, Y. Liu, N. Liu, Y. Han, X. Zhang, H. Huang, Y. Lifshitz, S.-T. Lee, J. Zhong, Z. Kang, Science 347 (2015) 970–974.
[2] J. Luo, J.-H. Im, M.T. Mayer, M. Schreier, M.K. Nazeeruddin, N.-G. Park, S.

D. Tilley, H.J. Fan, M. Grätzel, Science 345 (2014) 1593–1596.
[3] R. Sathre, C.D. Scown, W.R. Morrow, J.C. Stevens, I.D. Sharp, J.W. Ager, K. Walczak, F.A. Houle, J.B. Greenblatt, Energy Environ. Sci. 7 (2014) 3264–3278.
[4] R. Subbaraman, D. Tripkovic, D. Strmcnik, K.-C. Chang, M. Uchimura, A. P. Paulikas, V. Stamenkovic, N.M. Markovic, Science 334 (2011) 1256–1260.
[5] S. Bai, C. Wang, M. Deng, M. Gong, Y. Bai, J. Jiang, Y. Xiong, Angew. Chem. Int. Ed. 53 (2014) 12120–12124.
[6] Q. Liu, J. Tian, W. Cui, P. Jiang, N. Cheng, A.M. Asiri, X. Sun, Angew. Chem. 126 (2014) 6828–6832.
[7] E.J. Popczun, J.R. McKone, C.G. Read, A.J. Biacchi, A.M. Wiltrout, N.S. Lewis, R. E. Schaak, J. Am. Chem. Soc. 135 (2013) 9267–9270.
[8] D.-Y. Wang, M. Gong, H.-L. Chou, C.-J. Pan, H.-A. Chen, Y. Wu, M.-C. Lin, M. Guan, J. Yang, C.-W. Chen, J. Am. Chem. Soc. 137 (2015) 1587–1592.
[9] M.S. Faber, R. Dziedzic, M.A. Lukowski, N.S. Kaiser, Q. Ding, S. Jin, J. Am. Chem. Soc. 136 (2014) 10053–10061.
[10] X. Zou, X. Huang, A. Goswami, R. Silva, B.R. Sathe, E. Mikmeková, T. Asefa, Angew. Chem. 126 (2014) 4461–4465.
[11] J. Deng, P. Ren, D. Deng, X. Bao, Angew. Chem. Int. Ed. 54 (2015) 2100–2104.
[12] Y. Ito, W. Cong, T. Fujita, Z. Tang, M. Chen, Angew. Chem. Int. Ed. 54 (2015) 2131–2136.
[13] Y. Zheng, Y. Jiao, Y. Zhu, L.H. Li, Y. Han, Y. Chen, A. Du, M. Jaroniec, S.Z. Qiao, Nat. Commun. 5 (2014).
[14] L. Liao, S. Wang, J. Xiao, X. Bian, Y. Zhang, M.D. Scanlon, X. Hu, Y. Tang, B. Liu, H. H. Girault, Energy Environ. Sci. 7 (2014) 387–392.
[15] H.B. Wu, B.Y. Xia, L. Yu, X.-Y. Yu, X.W.D. Lou, Nat. Commun. 6 (2015).
[16] D. Gopalakrishnan, D. Damien, M.M. Shaijumon, ACS Nano 8 (2014) 5297–5303.
[17] L. Liao, J. Zhu, X. Bian, L. Zhu, M.D. Scanlon, H.H. Girault, B. Liu, Adv. Funct. Mater. 23 (2013) 5326–5333.
[18] Y.H. Chang, C.T. Lin, T.Y. Chen, C.L. Hsu, Y.H. Lee, W. Zhang, K.H. Wei, L.J. Li, Adv. Mater. 25 (2013) 756–760.
[19] Y. Li, H. Wang, L. Xie, Y. Liang, G. Hong, H. Dai, J. Am. Chem. Soc. 133 (2011) 7296–7299.
[20] D. Kong, H. Wang, J.J. Cha, M. Pasta, K.J. Koski, J. Yao, Y. Cui, Nano Lett. 13 (2013) 1341–5303.
[21] C. Tsai, F. Abild-Pedersen, J.K. Nørskov, Nano Lett. 14 (2014) 1381–1387.
[22] T.F. Jaramillo, K.P. Jørgensen, J. Bonde, J.H. Nielsen, S. Horch, I. Chorkendorff, Science 317 (2007) 100–102.
[23] J. Xie, H. Zhang, S. Li, R. Wang, X. Sun, M. Zhou, J. Zhou, X.W.D. Lou, Y. Xie, Adv. Mater. 25 (2013) 5807–5813.
[24] H. Wang, Z. Lu, D. Kong, J. Sun, T.M. Hymel, Y. Cui, ACS Nano 8 (2014) 4940–4947.
[25] X. Zhang, F. Meng, S. Mao, Q. Ding, M.J. Shearer, M.S. Faber, J. Chen, R. J. Hamers, S. Jin, Energy Environ. Sci. 8 (2015) 862–868.
[26] J. Xie, J. Zhang, S. Li, F. Grote, X. Zhang, H. Zhang, R. Wang, Y. Lei, B. Pan, Y. Xie, J. Am. Chem. Soc. 135 (2013) 17881–17888.
[27] J. Deng, H. Li, J. Xiao, Y. Tu, D. Deng, H. Yang, H. Tian, J. Li, P. Ren, X. Bao, Energy Environ. Sci. 8 (2015) 1594–1601.
[28] W. Zhou, D. Hou, Y. Sang, S. Yao, J. Zhou, G. Li, L. Li, H. Liu, S. Chen, J. Mater. Chem. A 2 (2014) 11358–11364.
[29] Y. Yang, H. Fei, G. Ruan, C. Xiang, J.M. Tour, Adv. Mater. 26 (2014) 8163–8168.
[30] X. Ge, L. Chen, L. Zhang, Y. Wen, A. Hirata, M. Chen, Adv. Mater. 26 (2014) 3100–3104.
[31] L. Yang, W. Zhou, D. Hou, K. Zhou, G. Li, Z. Tang, L. Li, S. Chen, Nanoscale 7 (2015) 5203–5208.
[32] D. Hou, W. Zhou, X. Liu, K. Zhou, J. Xie, G. Li, S. Chen, Electrochim. Acta 166 (2015) 26–31.
[33] W. Zhou, K. Zhou, D. Hou, X. Liu, G. Li, Y. Sang, H. Liu, L. Li, S. Chen, ACS Appl. Mater. Interfaces 6 (2014) 21534–21540.
[34] M.A. Lukowski, A.S. Daniel, F. Meng, A. Forticaux, L. Li, S. Jin, J. Am. Chem. Soc. 135 (2013) 10274–10277.
[35] L. Yang, H. Hong, Q. Fu, Y. Huang, J. Zhang, X. Cui, Z. Fan, K. Liu, B. Xiang, ACS Nano (2015).
[36] S. Zhuo, Y. Xu, W. Zhao, J. Zhang, B. Zhang, Angew. Chem. 125 (2013) 8764–8768.
[37] L. Zhang, H.B. Wu, Y. Yan, X. Wang, X.W.D. Lou, Energy Environ. Sci. 7 (2014) 3302–3306.
[38] S. Peng, L. Li, S.G. Mhaisalkar, M. Srinivasan, S. Ramakrishna, Q. Yan, ChemSusChem 7 (2014) 2212–2220.
[39] P. Leidinger, R. Popescu, D. Gerthsen, C. Feldmann, Chem. Mater. 25 (2013) 4173–4180.
[40] P. Leidinger, R. Popescu, D. Gerthsen, H. Lunsdorf, C. Feldmann, Nanoscale 3 (2011) 2544–2551.
[41] S.-H. Wu, Y. Hung, C.-Y. Mou, Chem. Mater. 25 (2013) 352–364.
[42] W. Zhou, Z. Yin, Y. Du, X. Huang, Z. Zeng, Z. Fan, H. Liu, J. Wang, H. Zhang, Small, 9, (2013) 140–147.
[43] X. Sun, J. Dai, Y. Guo, C. Wu, F. Hu, J. Zhao, X. Zeng, Y. Xie, Nanoscale 6 (2014) 8359–8367.
[44] C.-B. Ma, X. Qi, B. Chen, S. Bao, Z. Yin, X.-J. Wu, Z. Luo, J. Wei, H.-L. Zhang, H. Zhang, Nanoscale 6 (2014) 5624–5629.
[45] M.-R. Gao, M.K.Y. Chan, Y. Sun, Nat. Commun. 6 (2015).
[46] L. Cheng, W. Huang, Q. Gong, C. Liu, Z. Liu, Y. Li, H. Dai, Angew. Chem. Int. Ed. 53 (2014) 7860–7863.
[47] F. Wang, J. Li, F. Wang, T.A. Shifa, Z. Cheng, Z. Wang, K. Xu, X. Zhan, Q. Wang, Y. Huang, C. Jiang, J. He, Adv. Funct. Mater. 25 (2015) 6077–6083.
[48] S. Xu, D. Li, P. Wu, Adv. Funct. Mater. 25 (2015) 1127–1136.

Linjing Yang received B.S. degree from Hebei University of Technology in 2014. She is pursuing her M.D. degree under the supervision of Dr. Weijia Zhou and Prof. Shaowei Chen in New Energy Research Institute, South China University of Technology (SCUT). Her research interests include electrocatalytic water splitting and oxygen reduction.

Dr. Weijia Zhou completed his Ph.D. at Shandong University in 2012. He was doing research at Nanyang Technological University (NTU) in 2011. Now, Dr. Zhou is an associate professor of New Energy Research Institute, School of Environment and Energy, South China University of Technology (SCUT), China. His research interests are related to the design and synthesis of functional materials and devices for new energy conversion and storage, including photo and electro-catalytic water splitting and supercapacitor.

Jia Lu received her B.S. degree at South China Agriculture University in 2013, and now she is a master degree candidate at South China University of Technology (SCUT) under the supervision of Dr. Weijia Zhou and Prof. Shaowei Chen. Her research interest includes metal embedded carbon hybrid catalysts for oxygen reduction reaction and electrochemistry of water splitting.

Dongman Hou obtained her B.S. degree from School of Chemistry and Chemical Engineering, South China University of Technology in 2013. She is now pursuing her Master Degree under the supervision of Professor Guoqiang Li and Dr Weijia Zhou, South China University of Technology. Her researches focus on the fabrication and application of flexible electrodes for highly efficient hydrogen evolution.

Yunting Ke has been studying in College of Environment and Energy, South China University of Technology (SCUT), since 2013. She is doing experiments under the supervision of Dr. Weijia Zhou in New Energy Research Institute. Her research interest is electro-catalytic water splitting.

Prof. Guoqiang Li received his PhD degree of materials science at Northwestern Polytechnical University, Xi'an, China, in 2004. Afterwards, he joined GE Global Research as an R&D scientist, and then carried out two postdoctoral research experiences in University of Tokyo (2005–2007) under the JSPS fellowship, and University of Oxford (2007–2010) under the Royal Society International Incoming Fellowship. He has been a full professor at South China University of Technology, China since 2010. Prof. Li has broad interests in synthesis of compound semiconductor materials and fabrication of relevant devices. He has published over 100 peer-reviewed articles and patented over 40 techniques.

Dr. Zhenghua Tang currently is an associate professor of New Energy Research Institute at South China University of Technology. He is also the recipient of Guangdong Natural Science Funds for Distinguished Young Scholar. He obtained his B.S. degree at Lanzhou University in 2005. He started his Ph.D. program since August 2007 in Department of Chemistry, Georgia State University, USA. After that, he conducted his postdoctoral training at Department of Chemistry, University of Miami from 2012 to 2014. He started his current position since August, 2014. His research focuses on noble metal nanoclusters, nanocatalyst, electrochemistry, and peptide based nanomaterials.

Prof. Xiongwu Kang received his B.Sc. degree in materials science and engineering from the University of Science and Technology of China in 2007, and Ph.D. degree in Chemistry from University of California, Santa Cruz in 2012. After finishing a postdoctoral appointment at Georgia Institute of Technology, he started his independent research in South China University of Technology in 2015 and is a professor in department of environment and energy. He is currently dedicated in the surface functionalization and electrocatalysis of metal nanoparticles

Dr. Shaowei Chen obtained a B.Sc. degree from the University of Science and Technology of China, and then went to Cornell University receiving his M.Sc. and Ph.D. degrees in 1993 and 1996. Following a postdoctoral appointment in the University of North Carolina at Chapel Hill, he started his independent career in Southern Illinois University in 1998. In 2004, he moved to the University of California at Santa Cruz and is currently a Professor of Chemistry. He is also an adjunct professor at South China University of Technology. His research interest is primarily in the electron transfer chemistry of nanoparticle materials.